Diffusive and directional intracellular dynamics measured by field-based dynamic light scattering

Joo, C.; Evans, C.L.; Stapanic, T.; Hasan, T.; de Boer, J.F.

published in
Optics Express
2010

DOI (link to publisher)
10.1364/OE.18.002858

document version
Publisher's PDF, also known as Version of record

Diffusive and directional intracellular dynamics measured by field-based dynamic light scattering

Chulmin Joo[1,2,4], Conor L. Evans[1], Thomas Stepinac[1], Tayyaba Hasan[1], Johannes F. de Boer[1,3]*

[1]*Wellman Center for Photomedicine, Harvard Medical School and Massachusetts General Hospital, Boston, Massachusetts 02114, U.S.A.*

[2]*Department of Mechanical Engineering, Massachusetts Institute of Technology, Cambridge, Massachusetts 02139, U.S.A.*

[3]*Department of Physics and Astronomy, VU University, De Boelelaan 1081, 1081 HV Amsterdam, The Netherlands*

[4]*cmjoo@alum.mit.edu*

**jfdeboer@few.vu.nl*

Abstract: Quantitative measurement of diffusive and directional processes of intracellular structures is not only critical in understanding cell mechanics and functions, but also has many applications, such as investigation of cellular responses to therapeutic agents. We introduce a label-free optical technique that allows non-perturbative characterization of localized intracellular dynamics. The method combines a field-based dynamic light scattering analysis with a confocal interferometric microscope to provide a statistical measure of the diffusive and directional motion of scattering structures inside a microscopic probe volume. To demonstrate the potential of this technique, we examined the localized intracellular dynamics in human epithelial ovarian cancer cells. We observed the distinctive temporal regimes of intracellular dynamics, which transitions from random to directional processes on a timescale of ~0.01 sec. In addition, we observed disrupted directional processes on the timescale of 1~5 sec by the application of a microtubule polymerization inhibitor, Colchicine, and ATP depletion.

OCIS codes: (170.1530) Cell analysis; (290.1350) Backscattering; (290.5820) Scattering measurements; (170.4500) Optical coherence tomography; (170.3880) Medical and biological imaging.

References and links

1. J. J. Tyson, K. Chen, and B. Novak, "Network dynamics and cell physiology," Nat. Rev. Mol. Cell Biol. **2**(12), 908–916 (2001).
2. R. B. Nicklas, "How cells get the right chromosomes," Science **275**(5300), 632–637 (1997).
3. J. Li, G. Lykotrafitis, M. Dao, and S. Suresh, "Cytoskeletal dynamics of human erythrocyte," Proc. Natl. Acad. Sci. U.S.A. **104**(12), 4937–4942 (2007).
4. S. Yamada, D. Wirtz, and S. C. Kuo, "Mechanics of living cells measured by laser tracking microrheology," Biophys. J. **78**(4), 1736–1747 (2000).
5. L. Deng, X. Trepat, J. P. Butler, E. Millet, K. G. Morgan, D. A. Weitz, and J. J. Fredberg, "Fast and slow dynamics of the cytoskeleton," Nat. Mater. **5**(8), 636–640 (2006).
6. R. P. Kulkarni, D. D. Wu, M. E. Davis, and S. E. Fraser, "Quantitating intracellular transport of polyplexes by spatio-temporal image correlation spectroscopy," Proc. Natl. Acad. Sci. U.S.A. **102**(21), 7523–7528 (2005).
7. K. M. Van Citters, B. D. Hoffman, G. Massiera, and J. C. Crocker, "The role of F-actin and myosin in epithelial cell rheology," Biophys. J. **91**(10), 3946–3956 (2006).
8. B. J. Berne, and R. Pecora, *Dynamic Light Scattering: With Applications to Chemistry, Biology, and Physics* (John Wiley, New York, 1976).
9. W. Brown, *Dynamic Light Scattering: The Method and Some Applications* (Clarendon Press, Oxford, 1993).
10. T. Tanaka, and G. B. Benedek, "Observation of protein diffusivity in intact human and bovine lenses with application to cataract," Invest. Ophthalmol. Vis. Sci. **14**, 449–456 (1975).
11. Y. Georgalis, E. B. Starikov, B. Hollenbach, R. Lurz, E. Scherzinger, W. Saenger, H. Lehrach, and E. E. Wanker, "Huntingtin aggregation monitored by dynamic light scattering," Proc. Natl. Acad. Sci. U.S.A. **95**(11), 6118–6121 (1998).
12. J. Peetermans, I. Nishio, S. T. Ohnishi, and T. Tanaka, "Light-scattering study of depolymerization kinetics of sickle hemoglobin polymers inside single erythrocytes," Proc. Natl. Acad. Sci. U.S.A. **83**(2), 352–356 (1986).

#118834 - $15.00 USD Received 21 Oct 2009; revised 17 Dec 2009; accepted 29 Dec 2009; published 27 Jan 2010

13. R. P. Singh, V. K. Jaiswal, and V. K. Jain, "Study of smoke aerosols under a controlled environment by using dynamic light scattering," Appl. Opt. **45**(10), 2217–2221 (2006).
14. I. Nishio, J. Peetermans, and T. Tanaka, "Microscope laser light scattering spectroscopy of single biological cells," Cell Biophys. **7**(2), 91–105 (1985).
15. A. Meller, R. Bar-Ziv, T. Tlusty, E. Moses, J. Stavans, and S. A. Safran, "Localized dynamic light scattering: a new approach to dynamic measurements in optical microscopy," Biophys. J. **74**(3), 1541–1548 (1998).
16. P. D. Kaplan, V. Trappe, and D. A. Weitz, "Light-scattering microscope," Appl. Opt. **38**(19), 4151–4157 (1999).
17. R. Dzakpasu, and D. Axelrod, "Dynamic light scattering microscopy. A novel optical technique to image submicroscopic motions. I: theory," Biophys. J. **87**(2), 1279–1287 (2004).
18. R. Dzakpasu, and D. Axelrod, "Dynamic light scattering microscopy. A novel optical technique to image submicroscopic motions. II: Experimental applications," Biophys. J. **87**(2), 1288–1297 (2004).
19. G. Popescu, T. Ikeda, R. R. Dasari, and M. S. Feld, "Diffraction phase microscopy for quantifying cell structure and dynamics," Opt. Lett. **31**(6), 775–777 (2006).
20. C. Joo, T. Akkin, B. Cense, B. H. Park, and J. F. de Boer, "Spectral-domain optical coherence phase microscopy for quantitative phase-contrast imaging," Opt. Lett. **30**(16), 2131–2133 (2005).
21. M. A. Choma, A. K. Ellerbee, C. Yang, T. L. Creazzo, and J. A. Izatt, "Spectral-domain phase microscopy," Opt. Lett. **30**(10), 1162–1164 (2005).
22. W. Choi, C. Fang-Yen, K. Badizadegan, S. Oh, N. Lue, R. R. Dasari, and M. S. Feld, "Tomographic phase microscopy," Nat. Methods **4**(9), 717–719 (2007).
23. H. Ding, Z. Wang, F. Nguyen, S. A. Boppart, and G. Popescu, "Fourier transform light scattering of inhomogeneous and dynamic structures," Phys. Rev. Lett. **101**(23), 238102 (2008).
24. W. Choi, C.-C. Yu, C. Fang-Yen, K. Badizadegan, R. R. Dasari, and M. S. Feld, "Field-based angle-resolved light-scattering study of single live cells," Opt. Lett. **33**(14), 1596–1598 (2008).
25. H. Ding, F. Nguyen, S. A. Boppart, and G. Popescu, "Optical properties of tissues quantified by Fourier-transform light scattering," Opt. Lett. **34**(9), 1372–1374 (2009).
26. C. Joo and J. F. de Boer are preparing a manuscript to be called "Theory for field-based dynamic light scattering microscopy."
27. A. F. Fercher, C. K. Hitzenberger, G. Kamp, and S. Y. El-Zaiat, "Measurement of intraocular distances by backscattering spectral interferometry," Opt. Commun. **117**(1-2), 43–48 (1995).
28. T. Wilson, *Confocal Microscopy* (Academic Press, 1990).
29. J. A. Izatt, M. R. Hee, G. M. Owen, E. A. Swanson, and J. G. Fujimoto, "Optical coherence microscopy in scattering media," Opt. Lett. **19**(8), 590–592 (1994).
30. Liposyn II Intravenous Fat Emulsion, Hospira Inc., *http://www.hospira.com/Files/TPN_Liposyn_II.pdf*.
31. A. Einstein, "On the Motion – Required by the Molecular Kinetic Theory of Heat – of Small Particles Suspended in a Stationary Liquid," Ann. Phys. **17**, 549–560 (1905).
32. S. Yazdanfar, and J. A. Izatt, "Self-referenced Doppler optical coherence tomography," Opt. Lett. **27**(23), 2085–2087 (2002).
33. S. Tang, C.-H. Sun, T. B. Krasieva, Z. Chen, and B. J. Tromberg, "Imaging subcellular scattering contrast by using combined optical coherence and multiphoton microscopy," Opt. Lett. **32**(5), 503–505 (2007).
34. P. Bursac, G. Lenormand, B. Fabry, M. Oliver, D. A. Weitz, V. Viasnoff, J. P. Butler, and J. J. Fredberg, "Cytoskeletal remodelling and slow dynamics in the living cell," Nat. Mater. **4**(7), 557–561 (2005).
35. G. Lenormand, J. Chopin, P. Bursac, J. J. Fredberg, and J. P. Butler, "Directional memory and caged dynamics in cytoskeletal remodelling," Biochem. Biophys. Res. Commun. **360**(4), 797–801 (2007).
36. T. Ichikawa, M. Yamada, D. Homma, R. J. Cherry, I. E. G. Morrison, and S. Kawato, "Digital fluorescence imaging of trafficking of endosomes containing low-density lipoprotein in brain astroglial cells," Biochem. Biophys. Res. Commun. **269**(1), 25–30 (2000).
37. I. Itzkan, L. Qiu, H. Fang, M. M. Zaman, E. Vitkin, I. C. Ghiran, S. Salahuddin, M. Modell, C. Andersson, L. M. Kimerer, P. B. Cipolloni, K.-H. Lim, S. D. Freedman, I. Bigio, B. P. Sachs, E. B. Hanlon, and L. T. Perelman, "Confocal light absorption and scattering spectroscopic microscopy monitors organelles in live cells with no exogenous labels," Proc. Natl. Acad. Sci. U.S.A. **104**(44), 17255–17260 (2007).
38. A. E. Desjardins, B. J. Vakoc, G. J. Tearney, and B. E. Bouma, "Backscattering spectroscopic contrast with angle-resolved optical coherence tomography," Opt. Lett. **32**(21), 3158–3160 (2007).
39. A. Wax, C. Yang, V. Backman, K. Badizadegan, C. W. Boone, R. R. Dasari, and M. S. Feld, "Cellular organization and substructure measured using angle-resolved low-coherence interferometry," Biophys. J. **82**(4), 2256–2264 (2002).
40. J. W. Pyhtila, and A. Wax, "Rapid, depth-resolved light scattering measurements using Fourier domain, angle-resolved low coherence interferometry," Opt. Express **12**(25), 6178–6183 (2004).

1. Introduction

Cells are highly dynamic systems that continuously undergo internal reconfiguration through random and/or coordinated molecular and mechanical responses [1]. Intracellular dynamics such as the transport of molecules and cargos, along with cytoskeleton rearrangements, are fundamental processes that support a broad range of functions such as cell migration and division. These intracellular processes are derived from, and often influence physiological conditions of the cells. Malfunction of molecular motors, for instance, is believed to be

#118834 - $15.00 USD Received 21 Oct 2009; revised 17 Dec 2009; accepted 29 Dec 2009; published 27 Jan 2010

responsible for incorrect distribution of chromosomes, one of the main signatures of Down syndrome [2], and aberrant dynamics of the actin cytoskeleton is a distinct characteristic of invasive and metastatic cancer cells [3]. Quantitative measurement of intracellular processes would thus aid in building a better understanding of the underlying mechanisms of cellular states and functions.

Conventional methods for quantifying structural dynamics in living cells have typically involved time course measurements of exogenous tracers conjugated to cellular structures [4–6]. By monitoring the position of the tracers, these techniques probe molecular and mechanical responses such as cytoskeleton rearrangement. However, the introduction of exogenous tracers is likely to perturb the processes of interest, and the limited lifetime and uncertainties in the connectivity of the tracers to the structures may hinder a reliable characterization of cellular processes at various timescales [7].

Dynamic light scattering (DLS) is a widespread optical technique used to measure the diffusive properties of scattering particles in suspension [8,9]. Owing to its non-invasiveness and high sensitivity to particle size distribution, DLS has extensively been utilized to study protein kinetics [10,11], biopolymer aggregation [12], and for environmental sensing [13]. DLS has been combined with microscopes to study the diffusive properties of biological and material specimens with high spatial resolution [14–18]. Yet, these methods to date have been based only on scattered light intensity, incapable of measuring directional transport dynamics with nanometer-level sensitivity.

Recent advances in quantitative phase microscopy techniques enabled accurate measurement of amplitude and phase of optical waves related to sample structures and dynamics [19–22]. The combination of these phase imaging techniques with field-based light scattering spectroscopy has been demonstrated, and used to examine structural changes of cells and tissues by measuring scattering signatures as a function of scattering angles [23–25]. While those methods allow for assessing the heterogeneity of the sample structures, the measurement of time-dependent diffusive and directional dynamics of biological specimens such as living cells have not been demonstrated.

Here, we describe microscopic field-based dynamic light scattering (F-DLS) as a label-free, non-invasive technique to measure localized diffusive and directional transport dynamics. F-DLS makes full use of the amplitude and phase of optical waves scattered from structures inside a microscopic probe volume. Temporal autocorrelation analysis on the complex-valued signals enables to obtain mean-squared displacement (MSD) and time-averaged displacement (TAD) of scattering structures. The MSD represents the time-averaged variance of scatterer displacements, which gives access to diffusive properties of samples such as diffusion coefficients. The TAD, on the other hand, offers a statistical means to measure directional transport dynamics of scattering structures. Combination of F-DLS with a high-resolution microscope therefore leads to a novel detection method capable of measuring dynamic features of biological specimens with high spatial resolution.

We have performed theoretical and numerical analysis on F-DLS measurement, as detailed in Ref [26]. As such, in this manuscript, we focus mainly on experimental verification and applications of F-DLS. We show the validity of F-DLS analysis based on the measurement of emulsion particles, and demonstrate F-DLS as a tool for characterizing localized intracellular dynamics inside human ovarian cancer cells (OVCAR-5s). We non-perturbatively observe the transition from random to directional intracellular processes on a timescale of ~0.01 sec, which have been reported and confirmed in other systems. The physiological importance of the directional processes on a timescale of 1~5 sec is further examined by monitoring their disruptions for Colchicine-treated and ATP-depleted cells. This study demonstrates the potential of the F-DLS technique in characterizing mechanical properties of dynamic systems, which ultimately could impact a broad range of biomedical applications.

#118834 - $15.00 USD Received 21 Oct 2009; revised 17 Dec 2009; accepted 29 Dec 2009; published 27 Jan 2010

2. Methods

2.1 Spectral-domain optical coherence phase microscopy (SD-OCPM)

Microscopic F-DLS involves the calculation of the temporal autocorrelation function of complex-valued field information scattered from a microscopic probe volume. To this end, it is critical to measure the optical field with high spatial resolution and phase stability. In order to achieve this, we employed a spectral-domain optical coherence phase microscope (SD-OCPM) [20,21], a confocal interferometric imaging technique capable of measuring the depth-resolved amplitude and phase distribution of a specimen.

The basic principle of SD-OCPM is identical to that of Spectral Domain Optical Coherence Tomography (SD-OCT), as detailed in Refs [20,21,27]. Unlike typical SD-OCT imaging, SD-OCPM employs the light reflected from a surface along the probe beam path as a phase reference. Such a common path interferometer has superior rejection of common mode phase noise, such as vibrations and thermal drifts, compared to the conventional interferometers with separate reference and measurement arms. In the present SD-OCPM (Fig. 1), the light reflected from the bottom surface of a coverslip serves as a reference, and the measurement light is back scattered from the focal volume inside the specimen. The depth-resolved reflectance and phase information is obtained by examining the amplitude and argument of the complex interference signal at each depth location, respectively.

In addition, in a fiber-based SD-OCPM implementation, the core in the single-mode fiber acts as a detection pinhole. Thus, while the lateral resolution is determined by focusing and collection optics as in confocal microscopy [28], the axial resolution of SD-OCPM is determined by the combination of confocal and coherence gates [29]. Since the confocal and coherence gates are independent physical confinements for the focal volume, their point-spread functions are multiplicative, leading to an improvement in the axial resolution [29].

2.2 SD-OCPM setup

A schematic of the SD-OCPM interferometer is depicted in Fig. 1. Unless specified otherwise, an 800 nm Kerr-lens mode-locked Ti:Sapphire laser with a full width at half maximum (FWHM) bandwidth of ~130 nm illuminated a single-mode fiber-based 2 × 2 coupler (Corning flexcore 780 fiber, AC Photonics, Inc.).

The beam emitted from the sample arm fiber was collimated by the collimator with a $1/e^2$ beam diameter of ~3.4 mm, passed through the galvanometer-driven scanners (Cambridge Technology, Inc., MA) employed for the lateral beam scanning, and introduced into an inverted microscope (Axiovert 200, Zeiss, Germany) through its back port. Inside the microscope, a beam expander magnified the beam diameter to overfill the back-aperture of the objective, thereby fully utilizing the numerical aperture (NA) of the microscope objective. A microscope objective (Plan-Apochromat, 20 × /0.75, Zeiss, Germany) was used to deliver the light onto specimen with measured lateral and longitudinal resolution of 0.42 μm and 2.0 μm in FWHM, respectively. The corresponding focal volume is estimated as ~2 femtoliter. The objective was mounted on a piezo-electric transducer (Physik Instrumente, P-725.2CL) that allowed scanning the focus in the axial direction.

The light back-reflected from the surfaces and structures along the probe beam path were re-coupled into the fiber interferometer, and subsequently detected by a spectrometer. We built a high-speed spectrometer to acquire the cross-spectral density of reference and sample light in the shot-noise limited regime [20]. The beam emitted by the detection arm fiber was collimated by a lens with a focal length of 100 mm, and incident on a transmission volume holographic phase grating (1200 lines/mm, Wasatch Photonics, Inc.) at the Bragg angle. The spectrally dispersed beams were then focused by a three-element air-spaced lens (Nikon, Japan) onto a CCD array of a 2048-element line scan camera (L-104k, Basler, Germany, 10 μm × 10 μm pixel size). The maximum read-out rate of the camera was 29 kHz and the acquired spectra could be transferred continuously to the host computer by CameraLink at a resolution of 10 bits/pixel. A frame grabber (PCI-1428, National Instruments) installed in the host computer managed the acquisition of spectra.

#118834 - $15.00 USD Received 21 Oct 2009; revised 17 Dec 2009; accepted 29 Dec 2009; published 27 Jan 2010

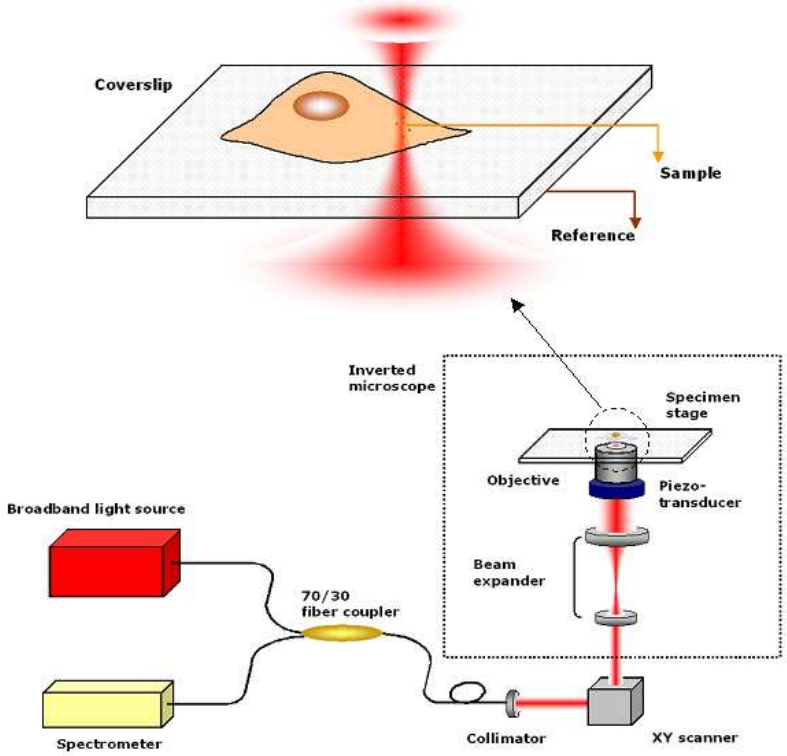

Fig. 1. Top: SD-OCPM detection scheme. SD-OCPM uses the light back-reflected from the bottom surface of a coverslip as a reference to ensure the phase stability in measuring amplitude and phase of sample light scattered from the focal volume. Bottom: A broadband light source illuminates a fiber-based common-path interferometer. The light coupled to the sample arm is delivered to a specimen via an integrated laser-scanning inverted microscope. The backscattered light is re-coupled to the fiber for the subsequent interference spectrum measurement at the detection arm.

2.3 F-DLS Analysis

The complex-valued depth-resolved information provided by SD-OCPM enables to locate the interference signal at a depth of interest inside a specimen. Given a time-varying signal, $F(t)$, a normalized temporal autocorrelation function is calculated as

$$R(\tau) = \frac{\left\langle F(t+\tau) F^*(t) \right\rangle}{\left\langle F(t) F^*(t) \right\rangle}, \tag{1}$$

where $\langle\ \rangle$ represents time-averaging operation, and τ denotes a temporal delay. The obtained normalized autocorrelation function is then regarded as a simple complex-valued exponential function given by [26]

$$R(\tau) \sim \exp(-\gamma_D Q_m^2 \sigma^2(\tau)) \exp(i\gamma_T \vec{\mu}(\tau) \cdot \vec{Q}_m). \tag{2}$$

Here, $\vec{Q}_m$ is the representative scattering vector, and γ_D and γ_T are the correction factors for diffusive and directional dynamics, that are introduced to correct the errors caused by the confocal detection (i.e., angular spectrum averaging due to high NA objectives). $\mu(\tau)$ and $\sigma^2(\tau)$ are the mean and variance of particle displacements. Based on our theoretical

#118834 - $15.00 USD Received 21 Oct 2009; revised 17 Dec 2009; accepted 29 Dec 2009; published 27 Jan 2010

analysis [26], we found that the model described in Eq. (2) is valid, and the diffusive and directional dynamics can be corrected by the proper scaling factors, γ_D and γ_T. The validity of this approximation will be further demonstrated through the experimental results in the subsequent section. Using Eq. (2), TAD and MSD along the direction of $\vec{Q}_m$ are calculated as:

$$\mu(\tau) = \frac{\tan^{-1}\left[\mathrm{Im}(R(\tau))/\mathrm{Re}(R(\tau))\right]}{\gamma_T Q_m}, \tag{3}$$

$$\begin{aligned} MSD(\tau) &= \sigma^2(\tau) + \mu^2(\tau) \\ &= -\frac{\ln\left(R(\tau)R^*(\tau)\right)}{2\gamma_D Q_m^2} + \left[\frac{\tan^{-1}\left[\mathrm{Im}(R(\tau))/\mathrm{Re}(R(\tau))\right]}{\gamma_T Q_m}\right]^2. \end{aligned} \tag{4}$$

Considering the back-scattering experimental configuration of SD-OCPM (Fig. 1), we use $\vec{Q}_m = (0,0,2k_0 n)$ as the representative scattering vector, where $k_0 = 2\pi/\lambda_0$ is the free-space wave number at the center wavelength λ_0 and n is the refractive index of a medium. The factor of 2 is due to the double-pass nature of the measurement. The TAD and MSD obtained in our analysis are thus related to the structure dynamics along the axial direction.

One should note that the TAD differs from the conventional Doppler shift or flow calculation in that it provides time-averaged statistical information. TAD comes from a correlation analysis, and provides statistical information on the mean displacement of scattering particles as a function of time-delay, not instantaneous flow. This is a result of a complex analysis (field-based analysis) of F-DLS, and is found to contribute to the MSD (Eq. (4). Statistical analysis through the calculation of a correlation function is well known to have much better immunity to noise components (e.g., rejection of autocorrelation noise). In the TAD calculation, the random fluctuations such as Brownian and instrument noise are averaged out, and so the determination of time-averaged directional motion (in the statistical sense, not instantaneous) can be made with sub-nanometer level sensitivity. For the MSD, it can be seen that it is composed of two terms related to the intensity fluctuation and directional motion. The first term is related to the random diffusion process, whereas the second term represents the convection or directional transport of scattering particles. This is different from the MSDs obtained by the conventional intensity-based DLS, where it measures only the contribution from the intensity fluctuation.

The ability to differentiate and examine the diffusive and directional dynamics in biological specimens is of great importance. For instance, biological materials such as biopolymers and cells undergo time-dependent changes in diffusive characteristics. Conventional DLS may not provide the information on whether these changes are due to conformational changes or directional motions. F-DLS enables to measure the random and directional dynamics separately, permitting a better understanding on the physical processes of the specimens of investigation.

2.4 Cells

Human epithelial ovarian cancer NIH: OVCAR-5 cells were obtained from the Fox Chase Cancer Institute (Philadelphia, PA, USA). Cells were plated on 35 mm collagen I-coated coverslip base dishes (MatTek Corp., Ashland, MA, USA) at a density of 5000 cells/cm^2 (less than 1/3 confluence). They were maintained at 37°C under a 5% CO_2 atmosphere in RPMI-1640 medium (Gibco Life Technologies, Grand Island, NY, USA) supplemented with 10% fetal bovine serum (FBS) (Gibco Life Technologies, Grand Island, NY, USA), and 1% 5,000 μg/ml penicillin streptomycin solution (Mediatech, Manassas, VA, USA).

#118834 - $15.00 USD Received 21 Oct 2009; revised 17 Dec 2009; accepted 29 Dec 2009; published 27 Jan 2010

2.5 Cell fixation

OVCAR-5 cells were plated at a density of 150,000 cells/ml on 35 mm collagen I-coated coverslip base dishes. The cells were incubated overnight in RPMI-1640 supplemented with 10% FBS and 1% 5,000 μg/ml penicillin streptomycin solution. Cells were then fixed for 15 minutes in 2% neutral buffered formalin in 1X PBS.

2.6 Colchicine treatment and ATP depletion

For Colchicine treatment, cells were incubated in 25 μM Colchicine (Sigma-Aldrich, St. Louis, MO) for 3 hours prior to measurement. ATP depletion was achieved by incubating the cells with 2 mM deoxyglucose and 2 mM NaN_3 (Sigma-Aldrich, St. Louis, MO) for 5 minutes prior to measurement. This incubation time was chosen to ensure the viability of the cells.

3. Results

3.1 SD-OCPM stability

We first measured SD-OCPM stability in order to understand the effect of instrument stability on F-DLS analysis. A collagen I-coated coverslip base dish was filled with a cell medium, and we measured the fluctuation of the interference between the reflections from the top and bottom surfaces of the coverslip. Figure 2a shows the experimental amplitude and phase fluctuation recorded at a sampling rate of 20 kHz, with the optical focus on the top surface of the coverslip. The phase stability was measured as ~9.8×10^{-3} rad at the measured SNR of ~37.5 dB. The theoretical prediction [20,21] at the SNR gives ~9.4×10^{-3} rad. Based on the measured fluctuations, F-DLS analysis was performed to obtain the magnitude of the autocorrelation function, MSD, and TAD (Figs. 2b-2d). The high stability of SD-OCPM provided a flat correlation function with a value of ~1, and the mean MSD and TAD were obtained as ~4.5×10^{-7} μm^2 and ~5.4×10^{-9} μm, respectively. This result demonstrates the high stability of SD-OCPM for accurate F-DLS analysis.

#118834 - $15.00 USD Received 21 Oct 2009; revised 17 Dec 2009; accepted 29 Dec 2009; published 27 Jan 2010

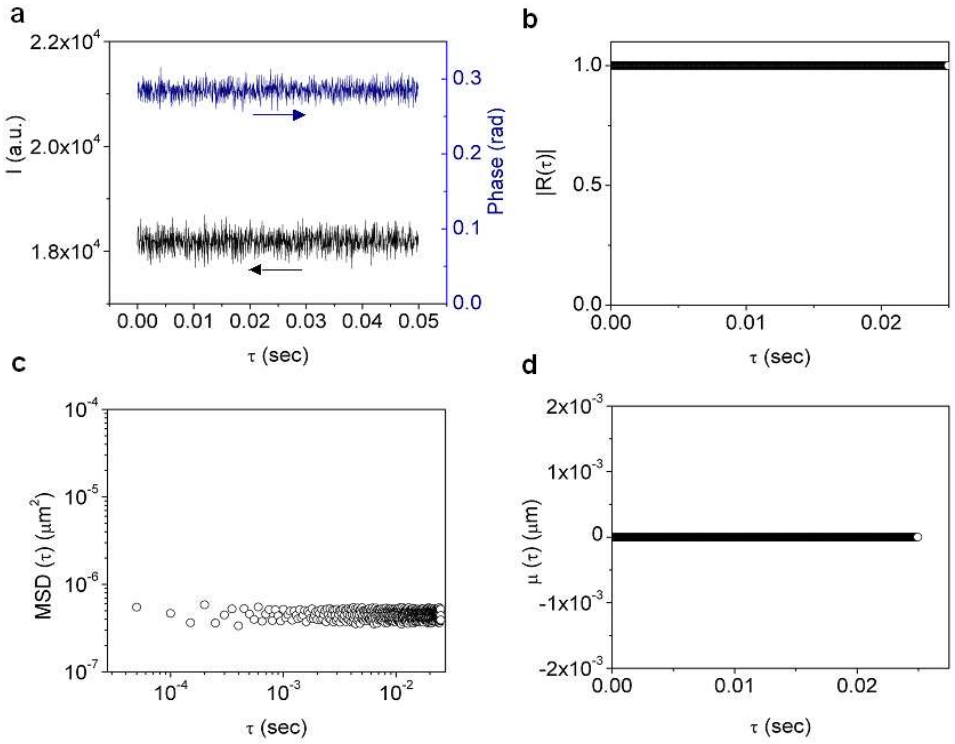

Fig. 2. (a) Measured amplitude and phase fluctuation of the interference between the reflected light from the top and bottom surfaces of a coverslip. The phase stability was measured as ~~9.8 × 10^{-3} rad at the measured SNR of ~37.5 dB. (b-d) Magnitude of the autocorrelation function, MSD, and TAD. The high stability of SD-OCPM produced a flat correlation with a value of ~1. The mean MSD and TAD were found as ~4.5 × 10^{-7} μm^2 and ~5.4 × 10^{-9} μm, respectively.

3.2 Brownian and directional motion of emulsion particles

The validity of our method was then assessed by examining the dynamics of emulsion particles (Liposyn, Hospira, Inc.), characterized by a nominal radius of ~200 nm [30]. For this validation experiments, a super-luminescent laser diode (SLD-371-HP2-DBUT-SM-PD, λ_0 ~840 nm, $\Delta\lambda_{FWHM}$ ~50 nm, Superlum, Ireland) and a 40 × /0.75 objective (UplanFL, Olympus, Japan) were used as the light source and as the focusing and collection lens, respectively. A 1% Liposyn solution in closed and flow chambers were used as a sample to model the particles undergoing Brownian and directional dynamics. A peristaltic syringe pump (11 Plus, Harvard Apparatus, Holliston, MA) induced the directional motion of the particles at volume flow rates (Q) of 80 μL /min and 160 μL/min. The optical axis of the probe beam was tilted by ~2.5 degrees relative to the flow direction. A coverslip-attached flow cell with a cross section area of ~7.5 mm^2 (Stovall Life Science, Inc., Greensboro, NC) was employed as the flow cell.

Figure 3a shows a depth-resolved SD-OCPM intensity distribution obtained with an optical focus at ~10 μm above the top surface of a base coverslip. As indicated by the red dot, the interference between the light scattered from the particles inside the focal volume and the light reflected from the bottom surface of the base coverslip could be easily identified due to the tightly focused optical beam with the high NA objective. We measured temporal fluctuation of that interference signal at a sampling rate of 20 kHz, and performed F-DLS analysis as described in the previous section. Figure 3b shows the magnitudes of the normalized autocorrelation functions for the particles in Brownian and directional motion, which presents shorter $1/e$ time constants for the higher volume flow rates. The MSDs were

#118834 - $15.00 USD Received 21 Oct 2009; revised 17 Dec 2009; accepted 29 Dec 2009; published 27 Jan 2010

evaluated assuming $\gamma_D = \gamma_T = 1$ (Fig. 3c), and fit with a power-law description (MSD ~$2D\tau^{\alpha}$). As expected, the exponent in the power-law fit to the static measurement produced ~1.04, which confirms Brownian motion of the particles. For the flow cases, a slight increase in the exponent is due to the contribution from the directional motion of the particles. The measured diffusion coefficients were ~0.99 μm^2/sec (Q = 0 μL/min), ~1.40 μm^2/sec (Q = 80 μL/min), and ~1.71 μm^2/sec (Q = 160 μL/min), respectively. Figure 3d shows the TADs extracted from the phase of the autocorrelation functions. The particles in the static measurement exhibited no net time-averaged displacement, as expected for Brownian particles. However, the directional motions in the flow measurements are represented by the linear TAD profiles with the measured time-averaged velocities of –6.4 μm/sec and –12.5 μm/sec, respectively.

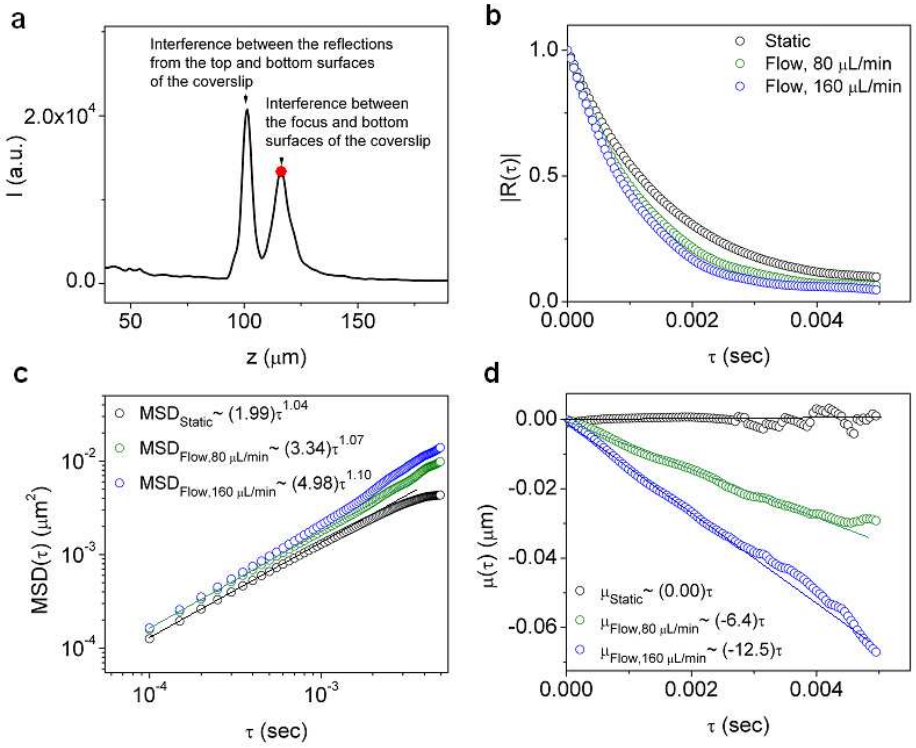

Fig. 3. F-DLS measurement for emulsion particles undergoing Brownian (black dot) and directional (green and blue dots) motion. The volume flow rates of 80 μL/min and 160 μL/min were used for the flow experiments. (a) SD-OCPM depth-resolved intensity distribution. The peak indicated by the red dot represents the interference between the light scattered from the emulsion particles inside the focal volume and the light reflected from the bottom surface of a coverslip. (b) Magnitudes of complex autocorrelation functions for the emulsion particles in Brownian and directional motion. The correlation function for the higher volume flow rate exhibits a shorter time constant. (c) MSDs: The power-law fits to MSDs found the exponents as ~1.04 for the particles in Brownian motion, and as ~1.07 and ~1.10 for the flow cases, respectively. The measured diffusion coefficient for the particles in Brownian motion (~0.99 μm^2/sec) agreed with the predicted value (~1.07 μm^2/sec) to within ~7%. (d) TADs calculated by the phase information of the complex autocorrelation functions. The static measurement exhibited no net time-averaged displacement, while the flow measurements showed linear behaviors with average velocities of –6.4 μm/sec (Q = 80 μL/min) and –12.5 μm/sec (Q = 160 μL/min), which agreed to the predicted values to within ~16% and ~20%, respectively.

The diffusion coefficient in our experiment on Brownian particles can be estimated theoretically based on the Stokes-Einstein equation given by $D = k_B T / 6\pi\eta a$ [31]. Here, k_B is the Boltzmann constant, T is the absolute temperature, η is the dynamic viscosity

#118834 - $15.00 USD Received 21 Oct 2009; revised 17 Dec 2009; accepted 29 Dec 2009; published 27 Jan 2010

of a medium, and a is the particle radius. Using the nominal size of the Liposyn particles (200 nm in radius) and the experimental conditions (T = 293 K throughout the experiments), we estimate the diffusion coefficient as ~1.07 μm^2/sec [32]. This agrees well with our experimental result for the static case (~0.99 μm^2/sec) to within ~7%. For the transport velocity estimation, the velocity along the channel can be simply estimated by dividing the used volume flow rate by the cross-sectional area of the flow cells. Taking into account the relative angle between the flow direction and optical axis, the flow velocities along the optical axis were found as –7.6 μm/sec for Q = 80 μL/min and –15.5 μm/sec for Q = 160 μL/min, respectively. These results suggest that our measured results correspond well to the predicted values to within ~16% and ~20%, respectively.

We note that the use of a high NA optics did not alter the exponents in the power-law description, since an exponent of ~1 was found in our measurements on the Brownian particles. Indeed, this result is consistent with our theoretical and numerical studies [26], where we found that the confocal detection with a high NA objective does not modify the exponents from ~1 for Brownian motion. However, the discrepancies in the diffusion coefficient and transport velocity between the actual values and measurement results may in part arise from the angular spectrum averaging due to the confocal detection. Through our analysis, those errors were found to depend on NA, and can be corrected by the proper scaling factors ($\gamma_D \sim \gamma_T \sim 0.93$ for 0.75 NA) [26]. Using these factors, the corrected MSD for Brownian particles produced a diffusion coefficient of ~1.06 μm^2/sec, which matches to the theoretically estimated value to within ~0.5%. The transport velocities obtained from the corrected TADs for the flow measurements were also found to be ~6.9 μm/sec (Q = 80 μL/min) and 13.4 μm/sec (Q = 160 μL/min), which now agree to the predicted values to within ~9% and ~13.3%, respectively.

3.3 Time-dependent intracellular dynamics

Having thus validated F-DLS measurements, we applied F-DLS to characterize dynamics of intracellular structures of live OVCAR-5 cells. In the experiments, we used a 0.75 NA objective (Plan-Apochromat, 20 × /0.75, Zeiss, Germany), and thus applied the correction factors accordingly, as discussed previously. Moreover, in order to focus on the time-dependent diffusive behaviors in cell dynamics, the exponent in the power-law fit was used as a descriptor in different temporal regimes.

The optical focal volume was positioned inside the cell cytoplasm at ~3.4 μm above the top surface of the base coverslip, and the back-scattered light was measured for ~26 seconds at a sampling rate of 5 kHz. During the measurement, all the scanners were stationary. A representative amplitude image of OVCAR-5s at that depth is shown in Fig. 4a. Highly scattering structures such as mitochondria, cytoskeletons, and other subcellular structures may contribute to the image contrast in SD-OCPM intensity image [33]. The amplitude and phase fluctuations recorded at the specified location in Fig. 4a are shown in Fig. 4b. We performed 62 measurements over 15 cells, and the summary of F-DLS analysis (the averages of log-transformed MSDs and magnitudes of TADs) is presented in Figs. 4c-4d. We show the results of F-DLS analysis upto $\Delta\tau$~6.5 sec because at the longer time delay, the number of data points for averaging is smaller, generating large errors. As can be noted, a transition from random to directional motion on a timescale of ~0.01 sec was observed for both the averages of the log-transformed MSDs and the magnitude of the TADs. The thickening of the average TAD profile is due to the large standard errors on the long timescales. Power-law fits to the MSDs ($MSD \sim \tau^{\alpha}$) on the short (1×10^{-4}~1×10^{-2} sec) and long timescales (1~5 sec) found the mean exponents to be 0.45 and 0.73, respectively ($p < 0.0005$). While the transition on this timescale can be attributed to many factors such as changes in the size of scattering structures, diffusive environment, and directional motion of the intracellular structures, TAD measurements (Fig. 4d) clearly show the presence and contribution from the directional motion of intracellular structures beginning around ~0.01 sec. These observations are consistent with previously reported results with exogenous tracers in terms of the transition

#118834 - $15.00 USD Received 21 Oct 2009; revised 17 Dec 2009; accepted 29 Dec 2009; published 27 Jan 2010

timescale between two distinctive dynamic regimes [34,35]. We also conducted 47 measurements over 10 fixed OVCAR-5 cells (Figs. 4e-4f). Compared with the measurements on the live cells, the fixed cells exhibited significantly different diffusive characteristics with the exponents of 0.25 and 0.22 on the short and long timescales. No directional motion of intracellular structures was observed, which validates the presence of directional processes in the live cells.

3.4 Effects of pharmaceutical interventions on intracellular dynamics

The molecular origin for the transition from random to correlated directional intracellular motion is known to be ATP-driven active transport, which is closely related to the physiological state and condition of the cells. To demonstrate the ability of F-DLS in measuring cellular responses to pharmaceutical interventions, we treated the OVCAR-5 cells with a microtubule polymerization inhibitor, Colchicine, and induced ATP-depletion, aimed at understanding the effect of microtubule-related and ATP-driven transport on the observed intracellular dynamics. Shown in Fig. 5a are the averages of log-transformed MSDs for the control ($N = 62$), Colchicine-treated ($N = 57$), and ATP-depleted cells ($N = 68$). The MSDs for the Colchicine-treated and ATP-depleted cells exhibited a larger offset on the short timescale, which is consistent with the observations made on these modified cells [5,7,34]. Power-law fits to the MSDs found that the mean exponents are 0.48 ± 0.01 and 0.47 ± 0.01 on the short timescale (1×10^{-4}~1×10^{-2} sec), and 0.54 ± 0.04 and 0.38 ± 0.02 on the long timescale (1~5 sec) for the Colchicine-treated and ATP-depleted cells, respectively (Figs. 5b-5c). The mean exponents on the short timescale (α) did not show a significant difference, but the exponents on the long timescale (β) for Colchicine-treated and ATP-depleted cells were found to be smaller by ~26% and ~48% compared to the control cells ($p < 0.0005$).

The TADs for the control cells exhibited coherent linear dynamics, but more randomized behaviors were observed for the Colchicine-treated and ATP-depleted cells (Fig. 5d). These randomized TADs were observed for all the measurements in Colchicine and ATP-depleted cells. However, the Colchicine-treated cells exhibited longer transition timescales from the linear to randomized dynamics than the ATP-depleted cells. We reasoned that the measured randomization might be due to disrupted directional motion by the pharmaceutical interventions. In order to validate our hypothesis, we examined the velocity correlation coefficients as a function of time-delay, $\Delta\tau$. If the intracellular dynamics are characterized by directional motion, the time-shifted velocity $v(\tau + \Delta\tau)$ should be correlated with $v(\tau)$, but no correlation should be observed for random motion. Figure 5e shows the velocity correlation coefficients between $v(\tau + \Delta\tau)$ and $v(\tau)$ as a function of $\Delta\tau$ averaged over all the measurements in each case. We found that the Colchicine-treated and ATP-depleted cells exhibited shorter time constants, with ~62% and ~84% decrease in directionality compared to the controls, respectively. These results suggest the importance of microtubule and ATP-driven processes for the directional intracellular transport in our measurements. The insets show the correlation diagrams at $\Delta\tau = 0.5$ sec in each case, demonstrating the disruption of directionality of intracellular motion by Colchicine and ATP depletion.

#118834 - $15.00 USD Received 21 Oct 2009; revised 17 Dec 2009; accepted 29 Dec 2009; published 27 Jan 2010

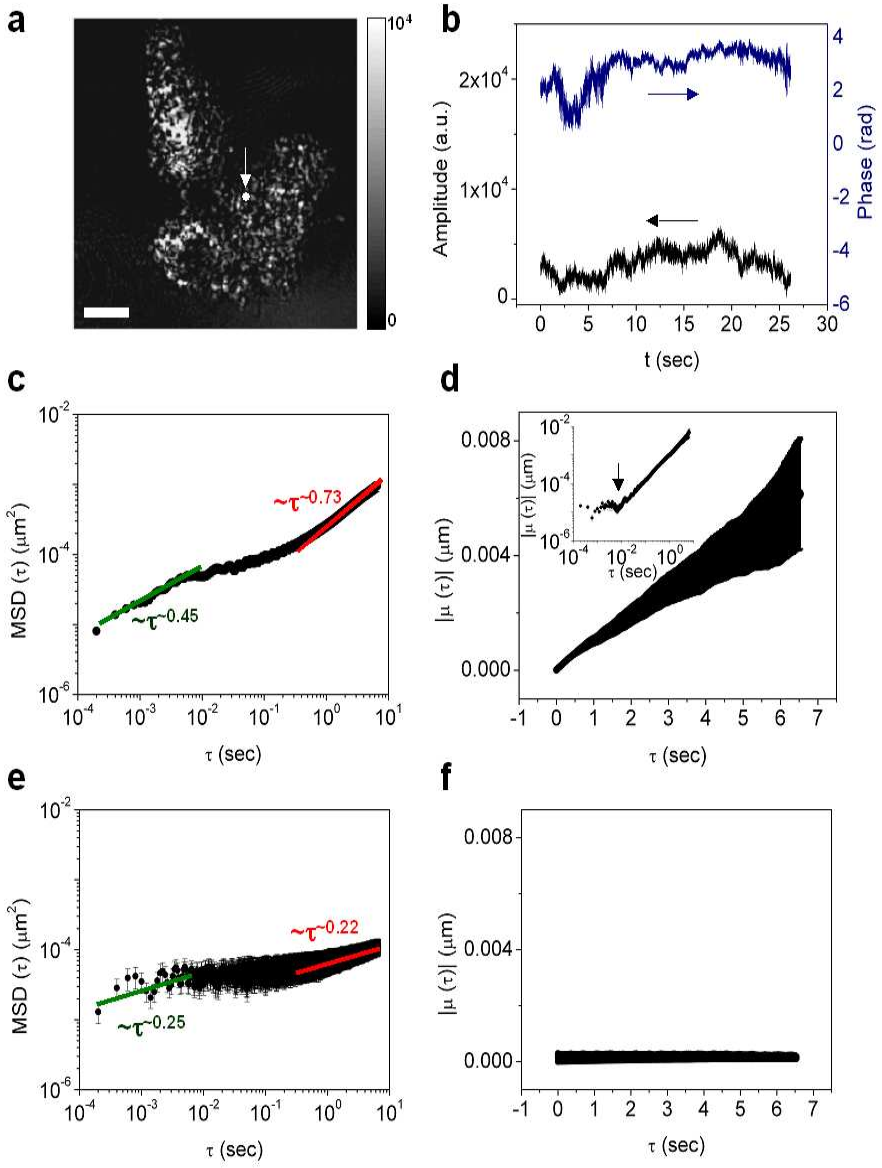

Fig. 4. F-DLS applied to monitoring intracellular dynamics of OVCAR-5 cells. (a) Representative amplitude image of the cells at a depth of ~3.4 μm above the top surface of the collagen-I coated coverslip. Highly scattering intracellular structures such as mitochondria and cytoskeleton may account for the observed image contrast. The scale bar denotes 10 μm. (b) Measured amplitude and phase fluctuation recorded at the position indicated in (a). (c-d) Summary of F-DLS analysis: averages of log-transformed MSDs and magnitudes of TADs (N = 62). The intracellular dynamics is shown to vary dramatically from random to directional processes at ~0.01 sec. The inset in (d) is the log-log plot of TAD for better visualization of the short timescale. The thickening of the average TAD profile is due to the large standard errors on the long timescales. (e-f) Averages of log-transformed MSDs and the magnitudes of TADs for the fixed cells (N = 47). The fixed cells exhibit significantly different diffusive characteristics with no directional transport. The error bar represents ± SE, and is included in (c-f).

#118834 - $15.00 USD Received 21 Oct 2009; revised 17 Dec 2009; accepted 29 Dec 2009; published 27 Jan 2010

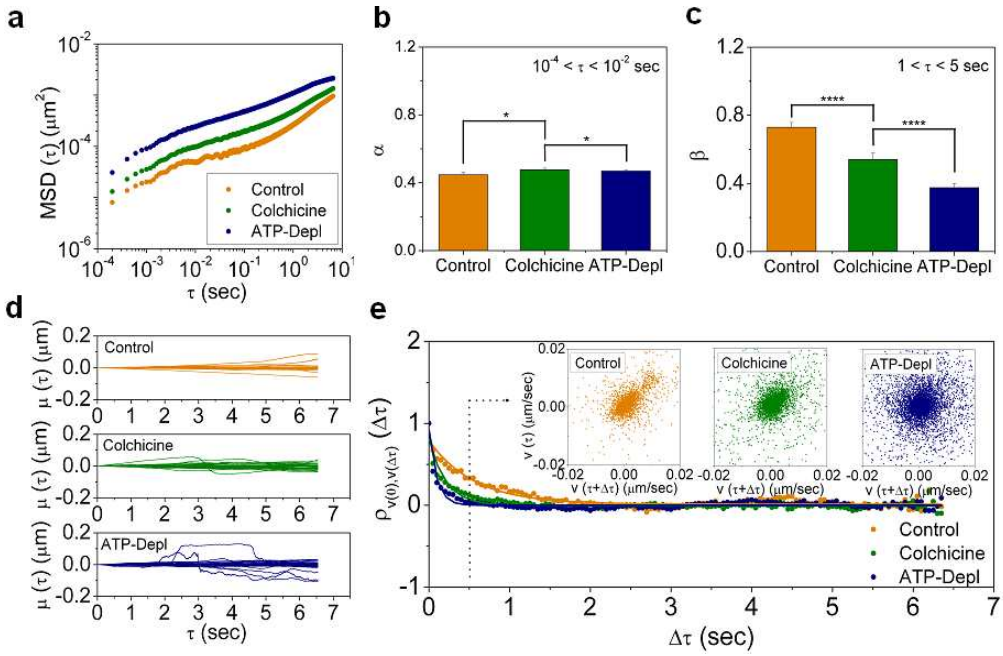

Fig. 5. Summarized F-DLS results for control (N = 62), Colchicine-treated (N = 57) and ATP-depleted (N = 68) OVCAR-5 cells. (a) Averages of log-transformed MSDs. (b-c) The mean exponents on the short timescale did not show a remarkable difference (*: p<0.5), but on the long timescale, the mean exponents for the control, Colchicine and ATP-depleted cells were 0.73, 0.54, and 0.38, respectively (****: p<0.0005). The error bar represents ± SE. (d) TADs: Most control cells exhibited directed motion as evident from the linear TAD profiles, whereas the Colchicine-treated and ATP-depleted cells showed randomized behaviors. (e) Velocity correlation coefficient as a function of time-delay, Δτ, averaged over all the measurements in each condition. The shorter time constants for Colchicine-treated and ATP-depleted cells indicate significant disruption of directional intracellular dynamics. The correlation diagrams at Δτ = 0.5 sec (inset) demonstrate the transition from correlated to randomized motion for Colchicine-treated and ATP-depleted cells.

4. Discussion

We presented the experimental demonstration of microscopic F-DLS based on SD-OCPM. Combined with its theoretical framework [26], F-DLS represents a quantitative method for measuring the diffusive and directional dynamics of biological samples inside a microscopic probe volume. In this manuscript, we experimentally validated F-DLS, and demonstrated its biological application to characterizing the intracellular dynamics of OVCAR-5 cells.

The intracellular structural dynamics of the OVCAR-5 cells were found to exhibit a distinction between short (up to ~0.01 sec) and long (1~5 sec) timescales, which is primarily due to the transition from random to directional intracellular motion. The existence of these distinctive temporal regimes is not unique to our system, with similar observations having been reported in the literature, mainly based on MSD analysis of micron-sized or fluorescent tracer particles [5,7,34]. The advantage of our method is that it permits quantitative measurements without the need for any exogenous tracers, while providing a means to differentiate the diffusive and directional intracellular processes. For the short timescales, the intracellular scattering structures undergo random and caged dynamics, and so the intracellular motion is primarily described by the diffusive motion. The enhanced diffusion on the timescale of 1~5 sec is a result of correlated motion of intracellular structures. At this timescale, the motion of the cytoskeleton, cargos, and other scattering intracellular structures are highly correlated and tend to move in the same direction. Using the TADs extracted from

#118834 - $15.00 USD Received 21 Oct 2009; revised 17 Dec 2009; accepted 29 Dec 2009; published 27 Jan 2010

F-DLS analysis, we directly observed the directional or correlated processes in intracellular motion, which is consistent with a recent report by Lenormand *et al.* [35]

The physiological significance of the directional intracellular motion in the cells was further studied by examining Colchicine-treated and ATP-depleted cells. Upon its introduction into the cells, Colchicine binds to tubulin, one of the main constituents of microtubules, to form a tight complex. The polymerization of this Colchicine-tubulin complex results in different morphology, which inhibits microtubule growth. Thus, it is expected to significantly hinder microtubule-dependent processes, such as the transport associated with kinesin and dynein. Based on our F-DLS analysis, and more specifically TAD results, a ~62% decrease in the velocity correlation coefficient was found compared to the untreated control cells, illustrating the importance of microtubules for directional intracellular transport in our measurements. As a more pronounced case, we performed the measurements on ATP-depleted cells. Though the relative short incubation time for ATP depletion did not seem to completely suppress all ATP-driven active transport, it was evident that those cells exhibit randomized behaviors, presenting ~84% decrease in terms of velocity correlation coefficient compared to the control cells. The importance and significant role of microtubule and ATP in intracellular directional motion have been investigated elsewhere [5,7,34]. However, it should be noted that most of the experimental approaches are based on tracers such as fluorescent makers and microbeads. F-DLS provides a label-free solution to localized intracellular dynamics investigation, which could find numerous applications in the long-term studies of cell dynamics without any perturbation to cell functions and states.

Comparison of our results to previously reported studies on intracellular transport and microrheology demonstrates a good agreement in the transition timescale between different dynamic regimes [34]. However, the exponents in the power-law fits and the average transport velocities obtained from our F-DLS analysis are different from those measured with conventional methods. The conventional methods such as particle tracking have reported the exponents of 0.5~0.8 on the short timescale and 1.2~1.6 on the long timescale [7]. Moreover, Kulkarni *et al.* [6] and Ichikawa *et al.* [36] measured an average velocity of ~50 nm/sec for the polyplex and endosomal transport inside the cells, respectively. Based on the theoretical analysis [26], we found that the observed sub-diffusive characteristics and lower transport velocities can be in part attributed to the heterogeneity in the structures and dynamics inside the probe volume. The scattered optical fields from the SD-OCPM focal volume arise from all the heterogeneous structures that may exhibit different diffusive and transport dynamics. Therefore, in contrast to the displacement of a single tracer particle in the conventional methods, the SD-OCPM signal is a result of coherent vector sum of the scattered optical fields from all the structures. As a result, the scattering strengths and concentrations of structures undergoing different dynamics would determine the exponents in MSD and the average velocities in TAD for F-DLS analysis. The larger transport velocity would correspond to a greater concentration of structures contributing to directionality along the same direction.

The combination of F-DLS analysis and SD-OCPM represents a new technique to measure localized diffusive and directional motions in dynamic systems. It provides a non-invasive and non-perturbative means to quantifying localized dynamics, and indeed demonstrated the observation of random and directional processes inside the living cells. Though coherent detection of back-scattered light does not offer structural specificity, recent advances in light-scattering spectroscopy [37] and angle-resolved detection methods [38–40] may offer specific information related to the composition of structures inside the probe volume.

Acknowledgements

This work was supported by grants from National Institute of Health (R01 RR19768, EY14975), the U. S. Department of Defense (F4 9620-01-1-0014), and the Center for Integration of Medicine and Innovative Technology. C. J. would like to thank the support through a Wellman Graduate Fellowship and a Hatsopoulos Innovation Award from the MIT Department of Mechanical Engineering.

#118834 - $15.00 USD Received 21 Oct 2009; revised 17 Dec 2009; accepted 29 Dec 2009; published 27 Jan 2010